

A. CZECH^{1*}, A. WRONA¹, M. LIS¹, M. KOT², Ł. MAJOR³

MICROSTRUCTURE CHARACTERIZATION OF REFRACTORY POWDER MATERIALS FOR LPBF METHOD

The primary goal of this study was to comprehensively characterize the microstructure of refractory powder materials, particularly molybdenum (Mo) and molybdenum-rhenium (Mo-Re), in both non-spherical and spherical forms. The characterization was carried out with the use of advanced techniques including scanning electron microscopy (SEM), transmission electron microscopy (TEM), energy dispersive spectroscopy (EDS) and nanohardness testing. This combination of analysis techniques provided a multi-scale understanding of the microstructural evolution and elemental distribution within the powders. Mo-Re powders were synthesized through powder metallurgy processes, while the spherical powders were produced with the use of the plasma spheroidization technique. Detailed analyses were conducted on the surface of powders, its cross-sections and thin foils. Spherical powders exhibited significant morphological changes, with evidence of rhenium diffusion within the molybdenum grain structure. This study provides detailed microstructural analysis of Mo-Re powders synthesized via plasma spheroidization, highlighting the role of rhenium in enhancing grain stability. The observed morphological changes in the spherical powders are indicative of enhanced material properties, which may influence their performance in critical applications. These findings provide valuable insights into the material properties, which may be crucial for demanding applications in high-temperature and high-stress environments, such as aerospace.

Keywords: Refractory metals; plasma spheroidization; SEM/TEM analysis; EDS analysis; additive manufacturing

1. Introduction

The most popular definition of refractory metal is an element of group 5 and 6, that has melting point higher than 2000°C. These are Nb, Mo, Ta, W, although some include Re from group 7 as well, as it do not fit in other classifications. Rhenium has a hexagonal closed packed structure, while refractory elements from groups 5 and 6 have body centered cubic (BCC) structure. It means that they have the strongest atomic bonds among other elements, which is unfortunate in their applications [1-3].

Due to unique properties such as high temperature strength, a growing interest in Mo applications is noticeable. It is widely applied in demanding environments like nuclear reactors or aerospace [4-7]. In general, high strength and low ductility in BCC metals are contributed to nonplanar core of screw dislocations. In molybdenum single BCC phase maintains from room temperature up to melting point [7]. Among several elements, that form solid solution with Mo, Re is an important alloying

addition. Elements with large atomic radius increase the recrystallization temperature. The solute atoms replace the solvent in the structure of Mo. The structure remains unchanged and the lattice parameter of the cubic unit cell changes with the content of solute. Since 1955, the so-called “Re effect” has been found to be beneficial in decreasing low temperature ductility within Group VIA metals, which have BCC crystal structure [4,7-13].

From a microstructural point of view there are few theories which may explain why adding rhenium is beneficial. The mechanism is not precisely known. The explanations include inducing non-planar core transfer to planar core that causes solid solution softening, promoting the formation of twin boundaries which brings more deformation in the material, electron concentration effect through reducing of oxygen content at grain boundaries or reducing Peierls stress [4,13,14].

Although the high cost of rhenium may be prohibitive, it is noticeable that, there is an increasing use of its additions in various applications [13,15].

¹ LUKASIEWICZ RESEARCH NETWORK – INSTITUTE OF NON-FERROUS METALS, 5 SOWIŃSKIEGO STR., 44-100, GLIWICE, POLAND

² AGH UNIVERSITY OF KRAKOW, FACULTY OF MECHANICAL ENGINEERING AND ROBOTICS, DEPARTMENT OF MACHINE DESIGN AND MAINTENANCE, AL. A. MICKIEWICZA 30, 30-059 KRAKOW, POLAND

³ INSTITUTE OF METALLURGY AND MATERIALS SCIENCE, POLISH ACADEMY OF SCIENCES, 25 REYMONTA STR., 30-059, CRACOW, POLAND

* Corresponding author: anna.czech@imn.lukasiewicz.gov.pl



The aim of this work was microstructural characterization of unmodified and rhenium-modified molybdenum powder, before and after the spheroidization process, intended for Laser Powder Bed Fusion (LPBF) technology. The analysis were performed by scanning and transmission electron microscopy techniques. To characterize the mechanical properties of the powders, nano-mechanical analyses were performed.

2. Materials and methods

In this study, four different powder materials were characterized:

- Commercially purchased, agglomerated, and sintered molybdenum (H.C. Stark, 99.4%, 15–45 μm);
- Agglomerated and sintered molybdenum with the addition of rhenium, manufactured at the Łukasiewicz Institute of Non-Ferrous Metals by classical powder metallurgy methods such as mechanical mixing and developed thermochemical reduction; as feedstock were used metallic molybdenum and ammonium perrhenate;
- Spherical molybdenum, manufactured at the Łukasiewicz Institute of Non-Ferrous Metals by plasma spheroidization method with the use of FST plasma system, 7MB torch, argon and hydrogen plasma gases;
- Spherical molybdenum-rhenium, manufactured at the Łukasiewicz Institute of Non-Ferrous Metals by plasma spheroidization method from prepared feedstock with the use of FST plasma system, 7MB torch, argon and hydrogen plasma gases.

The study involved surface morphology characterization, detailed microstructural analysis of cross-sections, qualitative chemical composition analysis and nanohardness testing.

Initially, a microstructural analysis of the powder surface morphology was performed using scanning electron microscopy (SEM) with the secondary electrons detector (SE). Subsequently, thin foils were prepared from individual non-spherical and spherical particles for cross-sectional transmission electron microscopy (TEM) analysis. This enabled detailed microstructural characterization in bright field mode (TEM BF), phase analysis using the selected area electron diffraction pattern (SAEDP) technique, and the generation of qualitative elemental distribution maps via energy dispersive spectroscopy (EDS). The primary objective of these analyses was to determine the distribution of rhenium within the molybdenum structure.

SEM analyses were conducted using a secondary electrons in-lens detector (Trinity-T2) on a DualBeam SCIOS II microscope (ThermoFisher). Due to the focus on surface morphology, a low accelerating voltage of 2 kV was selected. The same microscope was used for preparing thin foils for TEM analysis. The DualBeam microscope, in addition to the electron column for imaging, is equipped with an ion column, where a gallium (Ga^+) ion beam is used for preparing TEM thin foils from spe-

cific areas of interest. The preparation process is fully automated using the AutoTEM 4 software.

TEM analyses were carried out in bright field mode (TEM BF) and scanning-transmission mode (STEM). Phase analysis was performed using selected area electron diffraction (SAEDP) technique, while qualitative chemical composition was analyzed via EDS. Qualitative analysis on the powders surface was conducted using the JXA-8230 X-ray microanalyzer (JEOL) equipped with wavelength dispersive (WDS) and energy dispersive (EDS) spectrometers. This device allows for observation, testing, and identification of microstructural elements, as well as chemical composition analysis within micro-regions of 1 μm in metallic, ceramic, and organic materials.

Finally, the nanohardness of powders was examined. For this purpose, metallographic samples were prepared by embedding the powders in resin, followed by grinding with SiC papers and polishing with diamond suspension on cloth to obtain cross-sections. These prepared samples were then subjected to nanohardness testing using a nanoindenter. The aim of the analyses was to determine the effect of structural changes on mechanical properties at the nano-scale, such as nanohardness and Young's modulus. Tests were performed using the Anton Paar Step 500 device, equipped with Nanoindenter NHT3 (Nano Hardness Tester) and MCT3 (Micro Combi Tester) heads, which include a system for collecting and archiving measurement results. The NHT3 meets the requirements of the ASTM-E2546 standard for nanohardness testers, while the MCT3 module complies with ASTM standards C1624, E2546, G171, and ISO standards 14577, 20502, and 27307. The tests we carried out with a load of 5 mN. The maximum penetration depth was up to 300 nm.

3. Results and discussion

3.1. Molybdenum non-spherical powder microstructure characterization

The commercial non-spherical powder, as intended, consisted of individual Mo flakes (Fig. 1) Then, thin foils were prepared from a single non-spherical particle for cross-section TEM analysis. Microstructural characterization of the powder before the spheroidization process, performed on the cross-section, showed the presence of numerous pores. It was most likely open porosity, as suggested by SEM analyses. TEM analyses on a cross-section are two-dimensional analyses and three-dimensional features cannot be determined on their basis. The average size of individual powder grains was at the level of 40 μm Single crystallites were large enough to enable electron diffraction from individual grains (point diffraction – single crystal) (Fig. 2). EDS analysis showed the presence of a thin oxide layer (about 0.1 μm) on the powder flakes surface and within the pores (Fig. 3).

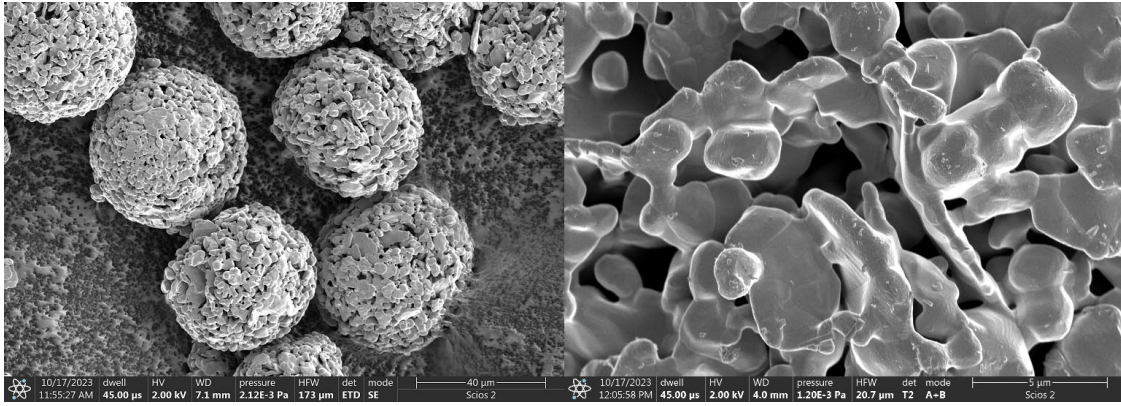


Fig. 1. SE electron images of Mo non-spherical powder, mag. $\times 1.2$ k & $\times 10$ k

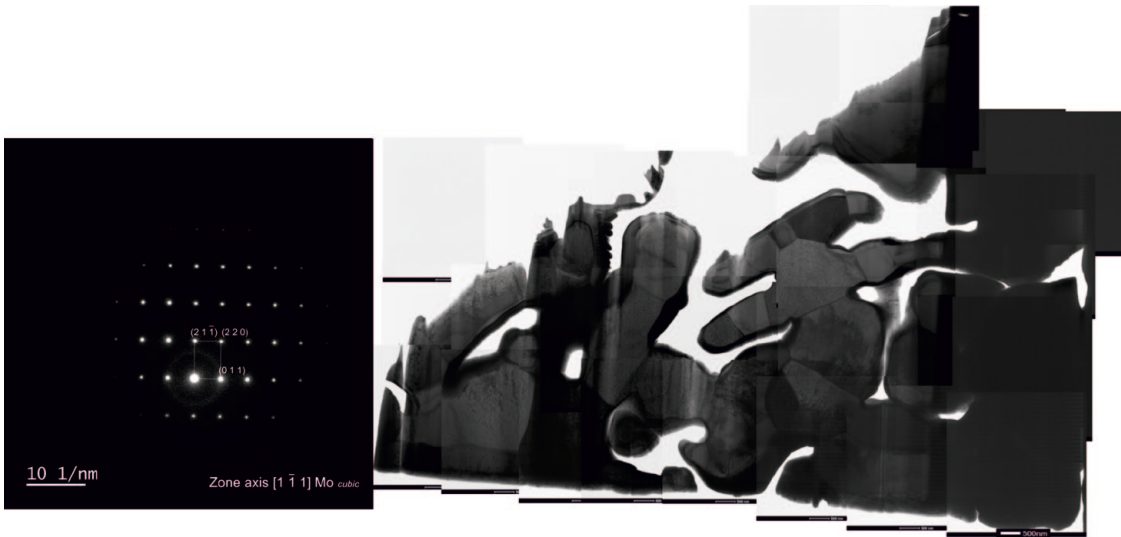


Fig. 2. TEM BF image & SAEDP pattern of Mo non-spherical powder



Fig. 3. STEM image & EDS element map distribution of Mo non-spherical powder

3.2. Molybdenum spherical powder microstructure characterization

Non-spherical Mo powder, of which the microstructure was described in the above subsection, were subjected to the spheroidization process. Its morphology changed from granules to uniform, spherical shape. (Fig. 4). The microstructural characterization of the surface topography was performed similarly to that

of the non-spherical Mo powder, using the SEM SE technique.

Microstructural characterization of the powder performed on the cross-section by TEM BF showed, that the pores were closed in the result of the spheroidization process (Fig. 5). Qualitative chemical analysis performed by EDS technique presented in the form of elemental distribution maps showed, that unlike the non-spherical powder, in the spherical Mo oxygen was practically unnoticeable (Fig. 6).

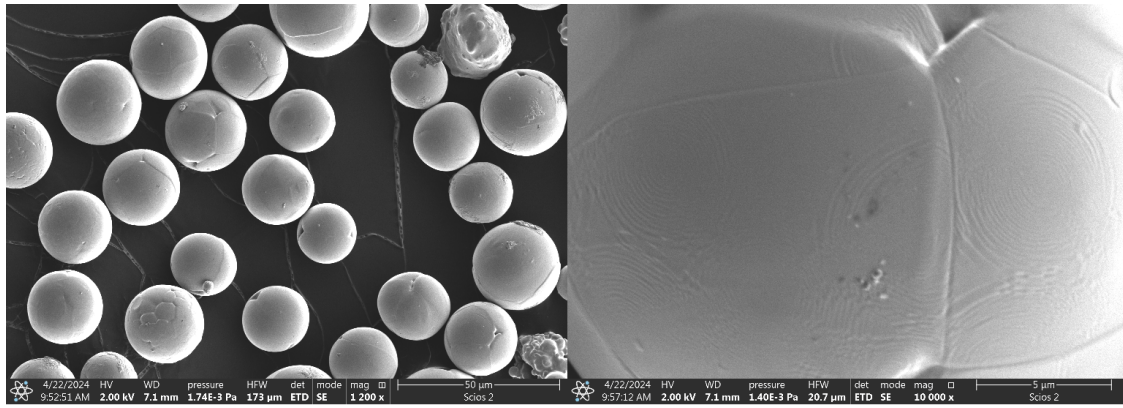


Fig. 4. SE electron images of Mo spherical powder, mag. $\times 1.2$ k & $\times 10$ k

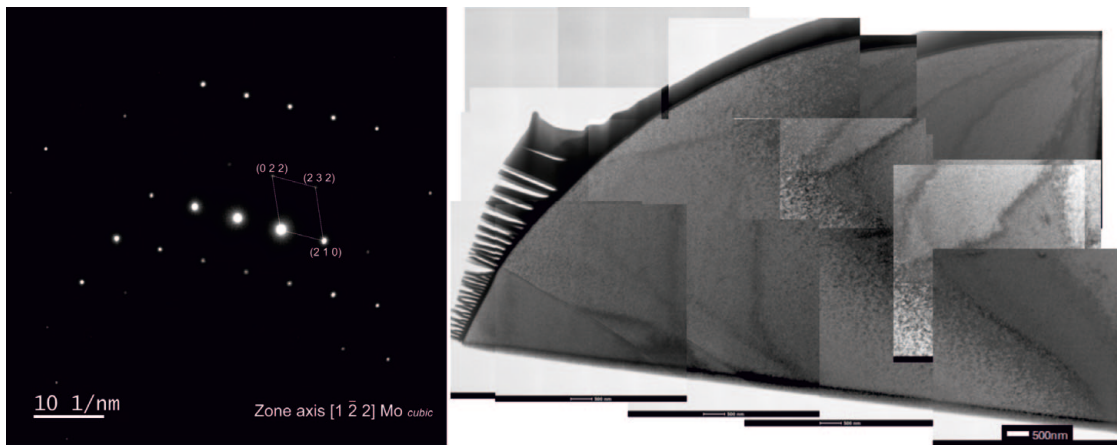


Fig. 5. TEM BF image and SAEDP of Mo spherical powder

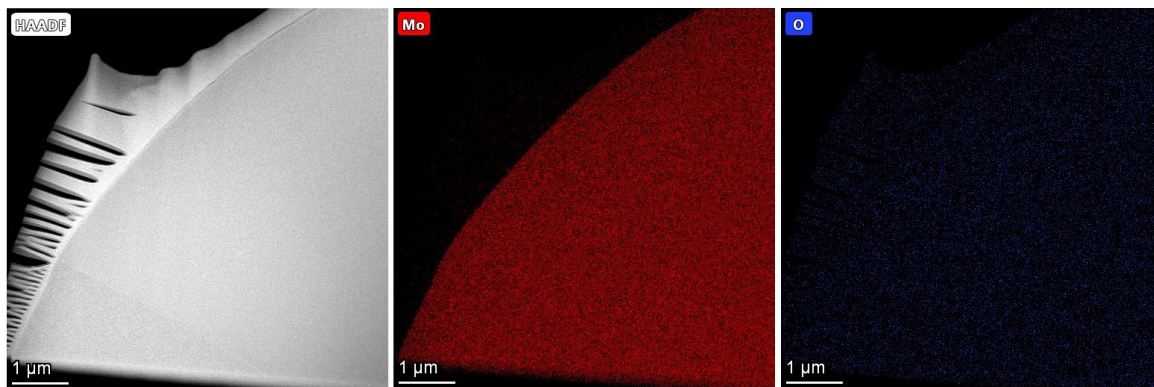


Fig. 6. STEM image & EDS element map distribution of Mo spherical powder

3.3. Molybdenum-rhenium non-spherical powder microstructure characterization

The non-spherical morphology of the Mo-Re powder differed slightly from that of the Mo powder which was shown in the SEM SE images. Although it consisted of flakes, they were more speckled (Fig. 7). The degree of porosity seemed to be much smaller. Small particles were also visible on the powder surface- Mo flakes were covered with metallic rhenium. The

distribution of rhenium varied depending on the type of powder. In the case of non-spherical powder, rhenium was distributed on its surface in the form of a thin (about 0.1 μm) layer which was presented in the cross-section using the TEM BF technique. Its structure was nano-crystalline as evidenced by the ring type of SAED (Fig. 8). It covered individual Mo flakes (Fig. 9). A thin layer of oxygen was characterized between the rhenium layer and the molybdenum particle, which may indicate the presence of molybdene oxide (Fig. 10).

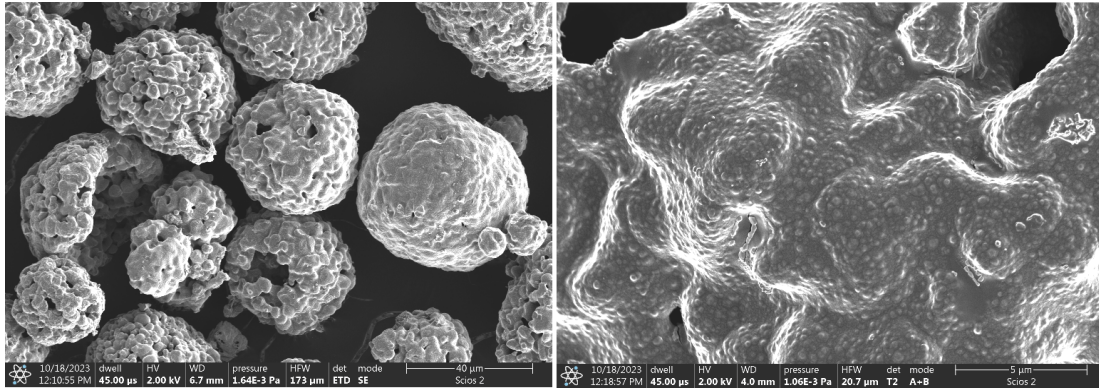


Fig. 7. SE electron images of Mo-Re non-spherical powder, mag. $\times 1.2\text{ k}$ & $\times 10\text{ k}$

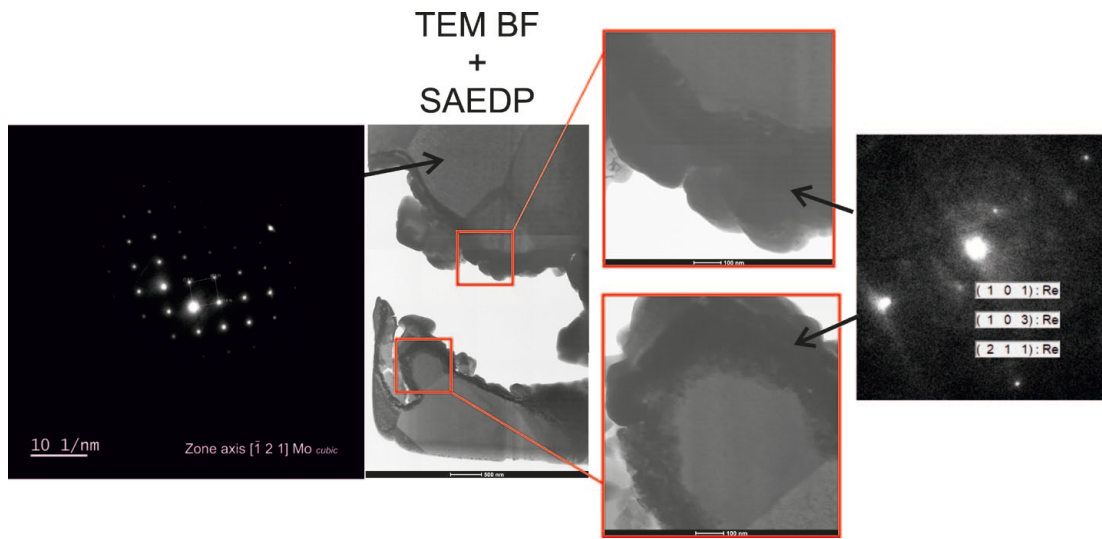


Fig. 8. TEM BF image & SAEDP pattern of Mo-Re non-spherical powder

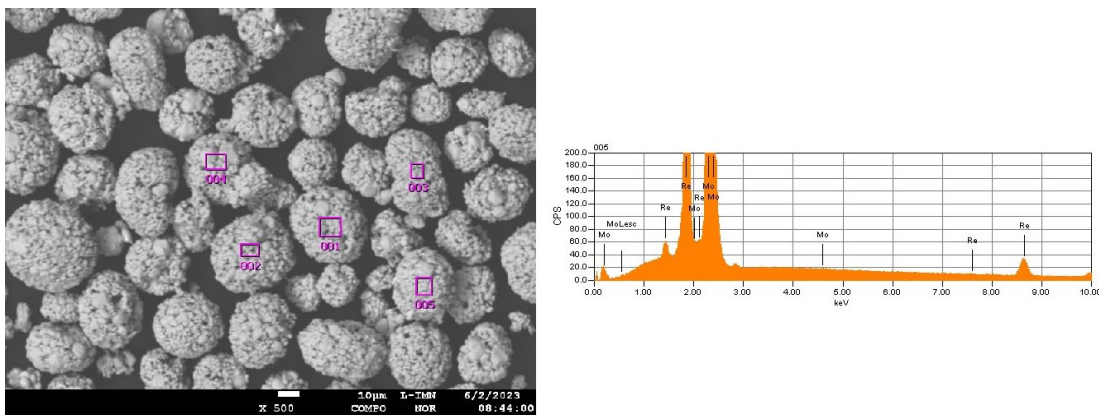


Fig. 9. Sample qualitative EDS analysis of Mo-Re non-spherical powder

3.4. Molybdenum-rhenium spherical powder microstructure characterization

After the spheroidization process, the morphology of the Mo-Re powder was changed to spheroidal (Fig. 11), it was similar to the spherical surface of pure Mo, which was shown in the cross-section in the SEM SE images. In the powder after spheroidization process, rhenium did not appear as a surface

layer. It was homogeneously distributed throughout the Mo-Re powder grain volume (Fig. 14). EDS qualitative analysis showed higher rhenium content in the granulated Mo-Re powder surface than in the spherical Mo-Re powder surface (Fig. 9, Fig. 13). It may indicate that after spheroidization process rhenium from the granule's surface was incorporated into the grain volume. During the spheroidization process, the MoRe cubic phase was probably formed (Fig. 12).

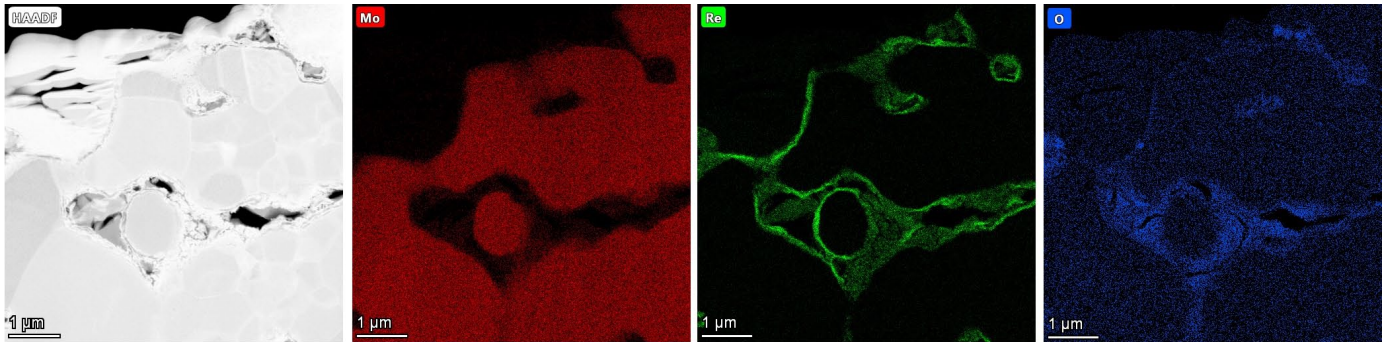


Fig. 10. STEM image & EDS element map distribution of Mo-Re non-spherical powder

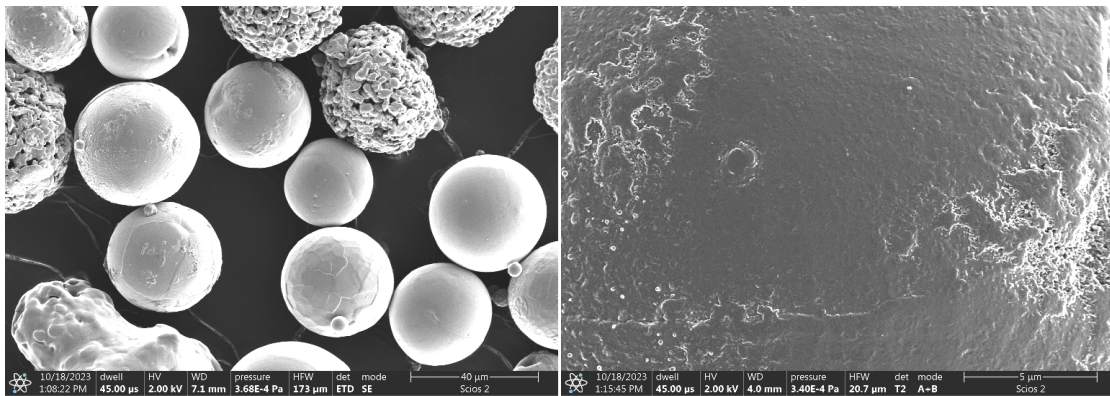


Fig. 11. SE electron images of Mo-Re spherical powder, mag. $\times 1.2\text{ k}$ & $\times 10\text{ k}$



Fig. 12. TEM BF image & SAEDP pattern of Mo-Re spherical powder

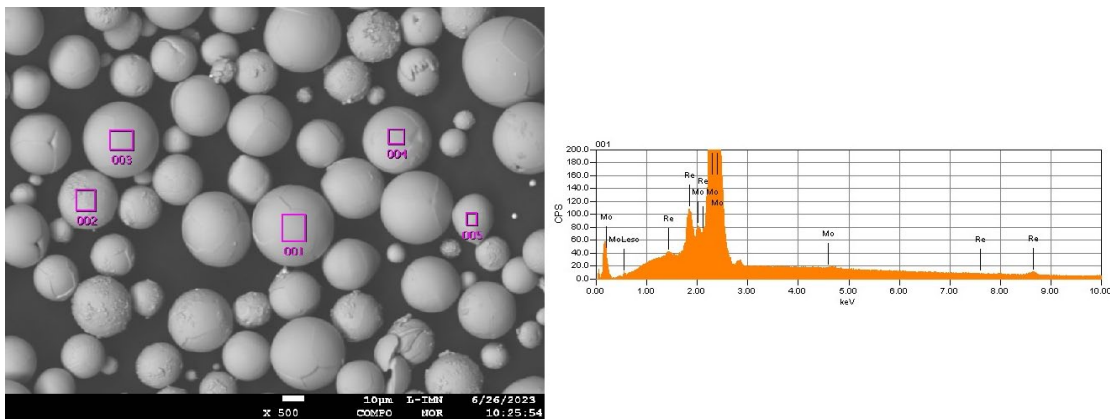


Fig. 13. Sample qualitative EDS analysis of Mo-Re spherical powder

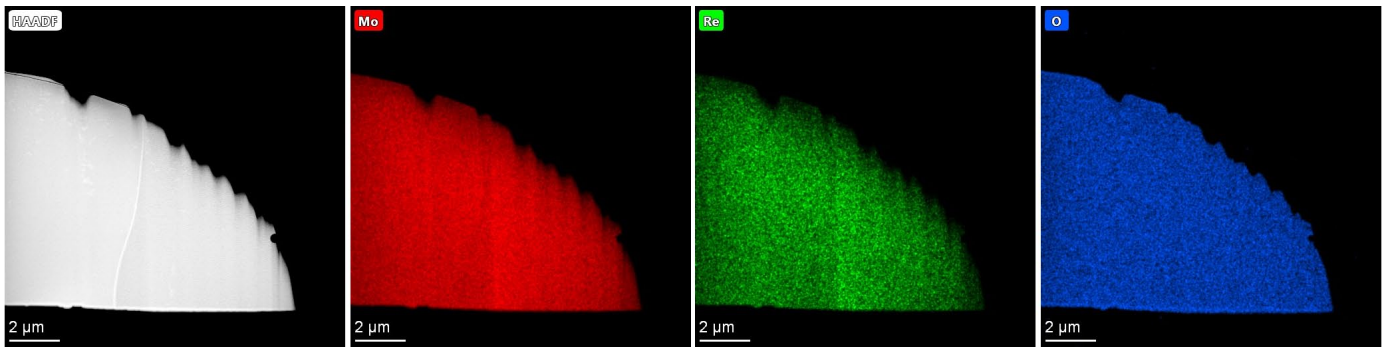


Fig. 14. STEM image & EDS element map distribution of Mo-Re spherical powder

3.5. Grain nanohardness & Young's modulus

Nanohardness results in a form of diagram with error ranges are presented in Fig. 15. The obtained traces were very small in relation to the grain size (average size approx. 40 μm). To avoid the influence of the resin on the measurement itself, measurements were taken from the center of powder grain. The scatter in the results may be the result of the heterogeneity of the powders and/or their porosity. Based on nanohardness results, the Young's modulus of tested materials was also calculated (Rys. 16). The analysis of deformation properties was based on the method of

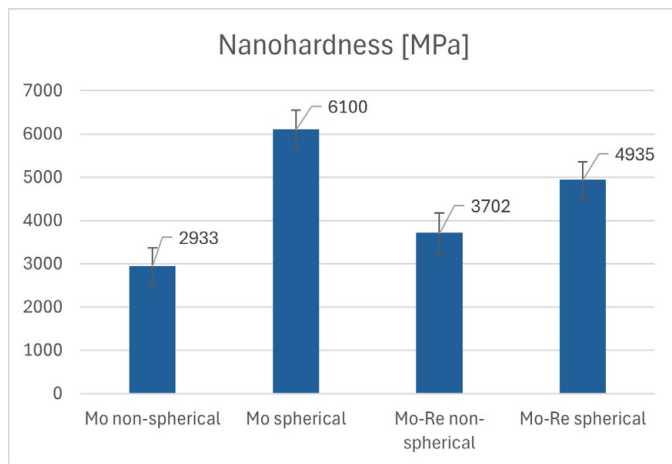


Fig. 15. Grain nanohardness diagram

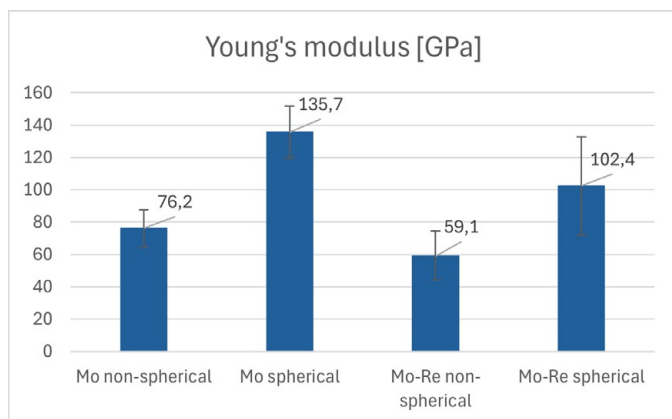


Fig. 16. Young's modulus diagram

Oliver and Pharr (Eq. 1), according to which the elastic modulus of the tested material is calculated directly from the obtained unloading curve:

$$E_r = \frac{\sqrt{\pi} \cdot S}{2 \cdot \sqrt{A}} \quad (1)$$

where:

E_r – reduced modulus of elasticity equal to

$$\frac{1}{E_r} = \frac{1-\nu^2}{E} + \frac{1-\nu_i^2}{E_i}$$

E, ν – Young's modulus and Poisson's ratio of the tested material;

E_i, ν_i – Young's modulus and Poisson number of the indenter material (for diamond $E = 1141$ GPa, $\nu = 0.07$);

S – contact stiffness (tangent of the unloading curve angle);

A – contact area taking into account permanent deformation.

Among tested materials, the highest nanohardness was achieved by Mo spherical powder and the lowest by non-spherical Mo powder. Spherical Mo-Re powder had lower value of nanohardness, which confirmed the fact that rhenium addition increases the plasticity of material. Interpreting obtained results for Mo-Re non-spherical powder, must be taken into account, that it consisted of two separate elements- rhenium formed a thin layer on molybdenum surface and that's why the results may be inaccurate.

4. Conclusion

Non-spherical Mo powder, as assumed, was characterized by a Mo (cubic) structure, the same as the Mo spherical powder. The plasma spheroidization process did not change the crystal structure of the material, but only changed its morphology from granulated flakes into spherical grains. In the non-spherical Mo-Re powder, two crystalline structures can be distinguished- Mo(cubic) and nano-crystalline Re. In turn, the Mo-Re spherical powder was characterized by a different crystal structure, it is probably MoRe(cubic). As with Mo powder, the morphol-

ogy was changed to spherical. Although plasma spheroidization process did not affected the crystal structure of Mo powders, it changed the crystal structure of Mo-Re powders. Rhenium transformed from the nanocrystalline form to the MoRe(cubic) form. Its distribution changed significantly, with its volume diffusion occurring within the Mo grain areas.

Volume diffusion of rhenium and probable MoRe (cubic) phase formation may cause the solid solution softening in spheroidized Mo-Re powder.

Micromechanical tests have indicated that the plasma spheroidization process, along with the associated rhenium volume diffusion, lead to a reduction in both hardness and Young's modulus. Specifically, for spherical Mo and Mo-Re powders, the Young's modulus decreased by over 30 GPa. This reduction may have positive implications in mitigating brittle fracture phenomena in molybdenum.

Acknowledgements

This work has been performed within the project: "Preparation and multi-scale characterization of materials from high-melting metals produced in the LPBF technology" Ministry of Science and Higher Education (pol. Ministerstwo Nauki i Szkolnictwa Wyższego) DWD/7/0210/2023

Powder materials were prepared within the project „Powder feedstock production and 3D printing of refractory metals and alloys for aerospace applications” M- ERA.NET2/2020/5/2021(11/PE/0220/21)

REFERENCES

- [1] W. Knabl, G. Leichtfried, R. Stickler, Refractory metals and refractory metal alloys. Springer Handbook of Materials Data, 307-337 (2018). DOI: https://doi.org/10.1007/978-3-319-69743-7_13
- [2] L. Northcott, Some features of the refractory metals. Journal of the Less Common Metals **3**, 2, 125-148 (1961). DOI: [https://doi.org/10.1016/0022-5088\(61\)90004-2](https://doi.org/10.1016/0022-5088(61)90004-2)
- [3] R.I. Jaffee, A brief review of refractory metals. Ohio, 1959.
- [4] R.L. Mannheim J.L. Garin, Structural identification of phases in Mo–Re alloys within the range from 5 to 95% Re. Journal of Materials Processing Technology **143**, 533-538 (2003). DOI: [https://doi.org/10.1016/S0924-0136\(03\)00342-X](https://doi.org/10.1016/S0924-0136(03)00342-X)
- [5] Y.J. Hwang, Y. Kim, S.H. Park, S.Ch. Park, K.A. Lee, Wear and Corrosion Properties of Pure Mo Coating Layer Manufactured by Atmospheric Plasma Spray Process. Arch. Metall. Mater. **69**, 1, 81-85 (2024). DOI: <https://doi.org/10.24425/amm.2024.147790>
- [6] W.J. Choi, Ch. Park, J. Buyn, Y.D. Kim, Fabrication of Molybdenum Alloy with Distributed High-Entropy Alloy Via Pressureless Sintering. Arch. Metall. Mater. **65**, 4, 1269-1272 (2020). DOI: <https://doi.org/10.24425/amm.2020.133682>
- [7] H. Xu et al., Mechanical and microstructural responses in molybdenum-rhenium alloys under hot compressions. Journal of Materials Research and Technology **30**, 3877-3885 (2024). DOI: <https://doi.org/10.1016/j.jmrt.2024.04.063>
- [8] P. Jéhanno, M. Böning, H. Kestler, M. Heilmaier, H. Saagem, M. Krüger, Molybdenum alloys for high temperature applications in air. Powder Metallurgy **51**, 2, 99-102 (2008). DOI: <https://doi.org/10.1179/174329008X313379>
- [9] K.J. Leonard, J.T. Busby, S.J. Zinkle, Microstructural and mechanical property changes with aging of Mo–41Re and Mo–47.5 Re alloys. Journal of Nuclear Materials **366**, 3, 369-387 (2007). DOI: <https://doi.org/10.1016/j.jnucmat.2007.03.027>
- [10] M. Osadnik et al., Plasma-sprayed Mo-Re coatings for glass industry applications. Surface and Coatings Technology **318**, 349-354 (2017). DOI: <https://doi.org/10.1016/j.surfcoat.2017.01.056>
- [11] J. Kim, R.E. Swanson, The role of Re additions on the grain size and the microstructure of Mo. Journal of Heat Treating **6**, 2, 111-115 (1988). DOI: <https://doi.org/0.1007/BF02833111>
- [12] J.L. Garin, R.L. Mannheim, Manufacturing of Mo-25 Re and Mo-50 Re alloys by means of powder sintering at medium temperatures. Material and Manufacturing Process **13**, 5, 731-747 (1998). DOI: <https://doi.org/10.1080/10426919808935295>
- [13] C.C Eckley et al., Evaluating Molybdenum-Rhenium Alloys Through Additive Manufacturing. JOM **75**, 6, 1928-1940 (2023). DOI: <https://doi.org/10.1007/s11837-023-05813-7>
- [14] T. Leonhardt et al., Investigation of mechanical properties and microstructure of various molybdenum-rhenium alloys. AIP Conference Proceedings **458**, 1, 685-690, American Institute of Physics (1999). DOI: <https://doi.org/10.1063/1.57638>
- [15] J.H. Schneibel, E.J. Felderman, E.K. Ohriner, Mechanical properties of ternary molybdenum–rhenium alloys at room temperature and 1700 K. Scripta Materialia **59**, 2, 131-134 (2008). DOI: <https://doi.org/10.1016/j.scriptamat.2008.02.057>